JOURNAL OF PROPULSION AND POWER
Vol. 10, No. 3, May–June 1994

Multiple Hole Ejector Performance with Short Wide Angle Diffusers

Kenneth C. Cornelius* and Gerald A. Lucius†
Wright State University, Dayton, Ohio 45435

The performance of a thrust augmenting ejector with multiple nozzle outlets for the primary jets is discussed. The addition of short diffusers at the end of the ejector and the utilization of the primary jets for boundary-layer control have resulted in a new high level of performance with a force augmentation greater than two. Diffusers having ejector length-to-mixing chamber diameter ratios of approximately (1.5–3.7) with diffuser half angles from (4.6–11 deg), and mixing chamber inlet area-to-primary nozzle area ratios of 36:1 and 72:1, were designed and tested. Additionally, a theoretical analysis of ejector performance was formulated. Comparisons between predicted and experimental performances as a function of the primary nozzle pressure ratio are discussed. Incomplete mixing and diffuser losses are measured and accounted for in a compressible control volume analysis. The data include selected experimental exit velocity profiles demonstrating the degradation of force augmentation at the higher pressure ratios.

Nomenclature

A_i = cross-sectional area, cm^2
A_r = diffuser area ratio A_4/A_3, Fig. 3
A_1 = primary jet fully expanded area to P_1, cm^2
A_1^* = primary jet throat area, cm^2
C_f = average skin friction coefficient
C_p = pressure coefficient normalized on P_a
D_3 = diameter of ejector, cm
F^* = normalized force $F/(P_aA_3)$
F_d = diffuser force from surface pressure, N
F_{ja} = isentropic jet force fully expanded to P_a, N
F_{j1} = isentropic jet force fully expanded to P_2, N
F_l = inlet lip force from surface pressure, N
F_{tx} = force of the ejector-jet combination, N
F_{vx} = force from skin friction, N
g = ratio of A_1/A_1^*
k = ratio of specific heats
L_i = length of ejector from jet exit, cm
M_i = Mach number $\sqrt{(kRT_i)}$
$\dot{m}_i$ = local mass flow rate at station i, kg/s
P_{cr} = critical pressure ratio for $M = 1$
P_i = static pressure, N/m^2
P_r = primary jet pressure ratio, nozzle plenum total/atm static
P_{rc} = primary jet local pressure ratio, nozzle plenum total/local static
P_{wi} = static pressure on wetted surface, N/m^2
P_{ti} = total pressure, N/m^2
R = ideal gas constant, kJ/kg K
s = entropy, kJ/kg K
T_i = static temperature, K
T_{ti} = total temperature, K
$\bar{V}_i$ = mean spatial velocity, m/s
x = longitudinal coordinate axis of model, cm
α = mass flow ratio, entrained flow/jet flow, $\dot{m}_2/\dot{m}_1$
β_i = momentum correction factor, $\int \rho V^2 \delta A_i/\dot{m}\bar{V}_i$
θ_e = diffuser effective half angle, deg
λ = ejector area to primary nozzle throat ratio, A_3/A_1^*
ρ = density of air, kg/m^3
ϕ = force ratio F_{tx}/F_{ja}, ejector/jet

Subscripts
a = atmosphere
e = exit
i = station identifier, defined in Fig. 3
j = jet

Received June 1, 1993; revision received Sept. 10, 1993; accepted for publication Sept. 15, 1993.

*Assistant Professor, Department of Mechanical and Materials Engineering.
†Graduate Student.

Introduction

THERE exists a large body of literature on ejectors for thrust augmentation. References 1 and 2 record the early efforts for the theoretical treatment of compressibility effects. In the open literature, work on supersonic ejectors[3–5] and the treatment of entrainment mechanisms for mixing are presented, and other references[6–9] report the effects of jet temperature and aeroacoustic interactions on the jet mixing rate. Recent advances in ejector performance include an overview on ejector theory[10] and a discussion of supersonic ejectors.[11] Additional augmentation is reported using diffusers[12] at the end of a straight ejector. A theoretical analysis[13] shows the ejector force augmentation degrading with forward flight speed. The previous research on single jet ejectors has concentrated on the capability of producing additional thrust at low speeds for takeoff of an aircraft, making an ejector configuration an attractive device for a V/STOL application. The criteria for using such a thrust system are that it must be of short length and provide significant thrust augmentation to yield a substantial net gain for a practical application.

Ejectors are purely pneumatic devices which transfer energy and impart motion to large quantities of ambient air. Unlike mechanical systems such as pumps or compressors which transfer energy through normal forces acting on the aerodynamic surfaces of rotating blades, ejectors transfer energy through turbulent shear stresses generated from the large eddies of the shear layer interfaces between the expanding jets and the entrained coflowing stream. Mixing jets in a closed environment of the ejector walls results in a mixing rate which differs from an unbounded environment. Freejet mixing occurs at a constant pressure, and the flux of momentum at any stage of the jet's development remains invariant. The jet spread rate is near linear beyond the potential core, and the centerline jet velocity decays according to an inverse power of distance. The jet spread rate parameter is a measure of the turbulent convection of momentum and the entrainment of the ambient fluid.

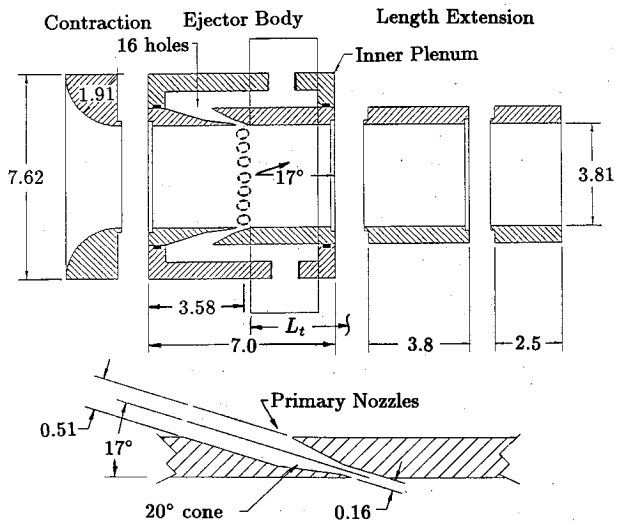

Fig. 1 Experimental ejector configuration, dimensions in centimeters.

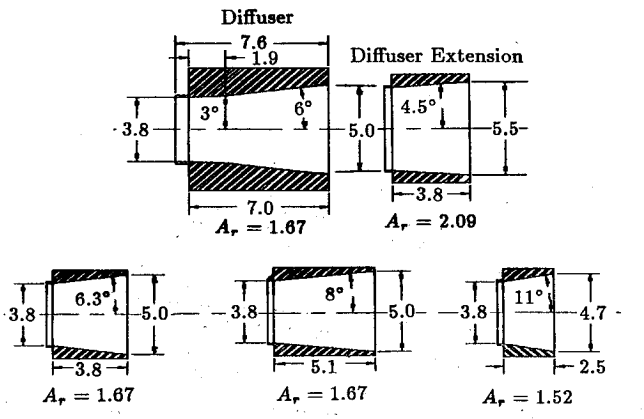

Fig. 2 Sketch of diffuser attachments, dimensions in centimeters.

A high-velocity fluid jet serves as the primary propulsive force which characterizes the source of energy. Mixing of the primary jet and the entrained stream of lower velocity in a confined region produces a reduction in the static pressure from ambient at the minimum cross section at the entrance to the ejector shown in Fig. 1. Therefore, confined mixing that occurs in ejectors has a strong adverse pressure gradient in the flow direction since the exit plane is at atmospheric pressure. The mixing process with these boundary conditions neglecting wall friction conserves total impulse (momentum flux plus pressure force) rather than the momentum flux for a free jet. In contrast to the free jet whose mass continuously increases with its development, the confined jet mixing develops downstream with the constraint that the mass flowing through any section of the mixing tube remains constant.

The action of the turbulent shear stress acting on the expanding high-velocity jet interface entrains ambient fluid which is accelerated through the contraction. Hence, additional thrust is produced by the reduced pressures acting on the upstream contoured lip surface of the inlet. This additional suction force generated from the entrained air as it accelerates into the duct provides the greatest augmentation of the primary propulsive force. The secondary entrained flow rate can be increased by connecting a diffuser at the end of the ejector straight section. The diffuser causes a further reduction in the duct pressure which increases the suction force on the inlet lip. It is somewhat of a departure from conventional thinking since useful thrust can be produced by an entropy producing mechanism.

The solution to the problem of reducing the length of ejectors without sacrificing performance includes devising a method to accelerate mixing between the primary and entrained streams. In the general case, all practical ejectors show improvements in performance when methods are found to accelerate mixing. The scheme for accelerating turbulent mixing for this study involves using multiple primary jet nozzles at the circumference of an ejector duct. The orientation of the jets in pitch and yaw at small angles to the axis of the ejector provides a swirl to the flow at the exit duct geometry. Unlike conventional ejectors where the plumbing for the primary jet is located inside the duct walls, the jets in this study are designed to exit from the duct wall, reducing the interference from the protruding hardware. The research focuses on the development of short ejectors with multiple jets to accelerate the mixing and study the performance characteristics of the overall ejector system.

Experimental Ejector Configuration

The following is a description of the experimental ejector configuration shown in Fig. 1. The ejector body was machined from aluminum in three segmented parts. The inlet section has a radius of curvature of 1.91 cm with a minimum cross-sectional diameter of 3.81 cm. A straight duct of length 7.0 cm was threaded to mate with the inlet. Sixteen holes of diameter 0.16 cm were drilled with equal spacing around the circumference through the wall of the inner duct section. The holes were drilled at complex angles with a pitch of 17 deg and clockwise yaw of 17 deg. A conical reamer was used to machine the holes to provide for a converging nozzle geometry for each jet. The holes penetrate the duct wall at a distance of 3.58 cm from the inlet of this section. As described earlier, the 16 pneumatic jets provide for the primary flow for the ejector and entrain secondary flow though the entrance for the purpose of thrust augmentation for the ejector assembly. The outer plenum consists of another circular section with the interior material volume milled out to provide for the passage of the compressed air to insure uniform total pressure for the primary jets around the circumference. Using a calibrated venturi, the discharge coefficient was measured as 0.93 at a total pressure ratio $P_r = 2.0$ and increased to 0.94 at $P_r = 7$ for the jet nozzles.

Duct extensions of different lengths shown in Fig. 1 were attached separately at the end of the ejector body to determine the optimum duct length for the force augmentation. Different area ratio diffusers with various lengths were also tested. Figure 2 shows a sketch of the diffuser attachments which could be individually screwed in at the rear of the ejector assembly. The entrance to the diffuser incorporates a smooth transition in wall angle. The θ_r ranged from 4.5–11 deg. The 17-deg yaw angle of the primary jets induces a swirl angle which imparts a net circulation in the clockwise direction for the mixed flow downstream.

A static pressure tap was installed at a distance of one duct diameter D_3 from the inlet of the ejector. This measurement provided for a calculation of the entrained mass flow $\dot{m}_2$ through the ejector. The mass flow was deduced by assuming uniform velocity across the constant diameter section and using the compressible flow equations for density and velocity. The compressed air line connected to a plenum which surrounds the ejector body. A pressure regulator provided variation of the total pressure yielding a range of P_r from 1.5 to 6.8. Pressure transducers were used for the plenum total pressure and measurement of the static pressures. A barometer was used for the measurement of the local atmospheric pressure.

Compressible Flow Analysis

The analysis in this section is for an ejector which transfers energy from the primary jets to the secondary stream in a mixing duct. The duct has a constant cross-sectional area terminated by a diffuser geometry. With the assumptions that the two compressible flows completely mix and that there are no pressure gradients normal to the mean flow direction, the equations can be algebraically solved. The compressible control volume analysis includes conservation of mass, momen-

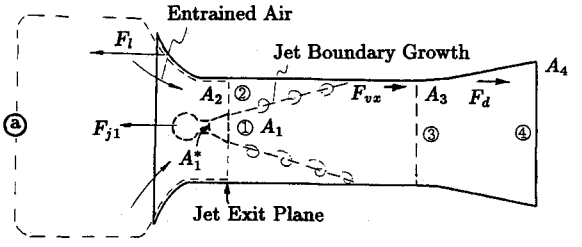

Fig. 3 Nomenclature for cross-sectional planes.

tum, and energy at downstream stations within the mixing duct. The solution provides an engineering estimate of the effect of geometric and fluid dynamic parameters on performance. For the theoretical analysis the nozzle was configured to have a converging-diverging geometry to the exit plane to extract the maximum thrust force above the critical effective pressure ratio, i.e., when the P_{re} becomes greater than critical, that is for

$$\left(P_r \frac{P_a}{P_2}\right) > \left(\frac{2}{k+1}\right)^{-k/(k-1)}$$

The analysis assumes that all variables are uniform at each cross-sectional area, which implies a totally mixed condition at the exit of station ③. Figure 3 shows the nomenclature for each cross-sectional plane. The equation of state for the thermodynamic variables is the ideal gas relationship. The flow is considered to be isentropic from atmospheric conditions to the duct entrance ⓐ to ②. The jet nozzle flow is assumed to expand isentropically from the plenum to the duct at station ② such that the static pressure is equal across the entire cross section, i.e., $P_1 = P_2$. The compressible control volume equations were formulated from Refs. 14 and 15. The analysis of the duct control volume between stations ② to ③ will be developed first, followed by an analysis of the diffuser between stations ③ to ④.

The continuity equation between stations ② to ③ is expressed as

$$\dot{m}_1 + \dot{m}_2 = \dot{m}_3, \qquad 1 + \alpha = (\dot{m}_3/\dot{m}_1) \tag{1}$$

where $\alpha = (\dot{m}_2/\dot{m}_1)$. The equation for the mass flow may be written and rearranged into the form

$$p_i A_i = \sqrt{\frac{R}{k}}\sqrt{T_{ti}}\frac{1}{M_i}\left(1 + \frac{k-1}{2}M_i^2\right)^{-(1/2)}\dot{m}_i \tag{2}$$

where $i = (1, 2, 3, 4)$. For the jet and entrained air, R and k are maintained as a constant value. The momentum equation, with the wall skin friction F_{vx}, may be written as

$$A_1 p_1(1 + kM_1^2) + A_2 p_2(1 + kM_2^2) - F_{vx} = A_3 p_3(1 + kM_3^2) \tag{3}$$

The enthalpy balance from the energy equation, assuming a constant specific heat and no heat transfer, and utilizing Eq. (1) applied from the jet exit plane to the end of the straight section from ② to ③, becomes

$$\frac{T_{t3}}{T_{t1}} = \frac{1 + \alpha(T_{t2}/T_{t1})}{1 + \alpha} \tag{4}$$

For flow at any plane the Mach number can be expressed in terms of the local stagnation pressure ratio as

$$M_i^2 = \frac{2}{k-1}\left[\left(\frac{P_{ti}}{P_i}\right)^{(k-1)/k} - 1\right] \tag{5}$$

Combining the conservation of mass Eq. (2) with the stagnation pressure definition Eq. (5), and applying them across the diffuser and assuming the flow is entirely mixed at the entrance to the diffuser, results in the following:

$$M_4\left(1 + \frac{k-1}{2}M_4^2\right)^{(-k-1)/2(k-1)} = \frac{1}{A_r}\left(\frac{P_{t3}}{P_{t4}}\right)M_3\left(1 + \frac{k-1}{2}M_3^2\right)^{(-k-1)/2(k-1)}\left(\frac{T_{t4}}{T_{t3}}\right)^{1/2} \tag{6}$$

The total pressure loss of the flow across the diffuser is expressed in terms of the inlet Mach number M_3, where the diffuser loss coefficient has the functional form $L_s = l(A_r, \theta)$. The entropy increase in terms of the diffuser loss coefficient is defined from $(s_4 - s_3)(1/R) = (L_s k M_3^2/2)$. The total pressure ratio from the outlet to the inlet which correlates with the entropy increase is expressed as

$$\frac{P_{t4}}{P_{t3}} = \exp(-L_s k M_3^2/2)\left(\frac{T_{t4}}{T_{t3}}\right)^{k/(k-1)} \tag{7}$$

The solution must satisfy the entropy equation where the turbulent viscous mixing provides for an entropy increase for the mixed flow downstream:

$$\dot{m}_3 s_3 - (\dot{m}_1 s_1 + \dot{m}_2 s_2) > 0 \tag{8}$$

The above equations can be solved using the known total temperatures which are equal and constant for this analysis at stations ② and ①, and therefore, constant across each station. For the ejector problem under consideration, $P_2 = P_1$ and $P_{t2} = P_a$. Choosing values of $(P_a/P_2) > 1$ at a given P_r until all the above equations are satisfied provides for the one-dimensional compressible solution. When $M_2 = 1$, the choked condition is maintained at the entrance and the calculation proceeds with (P_a/P_2) evaluated at the critical pressure ratio for the inlet flow. The performance parameters follow directly from the thermodynamic and flow variables, where the mass flow Eq. (2) for the entrained and jet flow rate is formulated in a ratio where $\alpha = (\dot{m}_2/\dot{m}_1)$, and is expressed as

$$\alpha = \left(\frac{\lambda}{g} - 1\right)\left(\frac{T_{t1}}{T_{t2}}\right)^{1/2}\left(\frac{M_2}{M_1}\right)\left(\frac{P_{t1}}{P_{t2}}\right)^{(1-k)/2k} \tag{9}$$

where $g = (A_1/A_1^*)$, the one-dimensional isentropic jet area expansion from the throat area to the duct static pressure P_2, which is a function[15] of the local pressure ratio P_{t1}/P_1 and the parameter $\lambda = (A_3/A_1^*)$ (ejector area/jet throat area).

From the momentum integral equation the thrust force in the axial direction of the ejector can be written in terms of the surface pressure integral, jet reaction, and skin friction force, and equated to the momentum flux plus an exit pressure difference term as

$$F_{tx} = \int (P_s - P_a)\,dA_x + F_{j1} - F_{vx} = \dot{m}_e V_{ex} + (P_e - P_a)A_{ex} \tag{10}$$

where the subscript e denotes the exit plane. The quantity of interest is the force ratio for an ejector with a straight pipe section or diffuser, and is defined from the left or right side of Eq. (10), where for this analysis $P_e = P_a$ at the exit plane. The ejector force is normalized by the nozzle reaction force F_{ja}, which is defined to be an isentropic expansion to the atmospheric static pressure,[15] neglecting the nozzle surface shear stress. This represents the maximum jet force that would

be obtained without the ejector body surrounding the nozzle. The force ratio is expressed as

$$\phi = \left(\frac{F_{tx}}{F_{ja}}\right) = \frac{(T_{te}/T_{t1})^{1/2}(1 + \alpha)[1 - (P_{te}/P_e)^{(1-k)/k}]^{1/2}}{[1 - P_r^{(1-k)/k}]^{1/2}} \quad (11)$$

The variables α and ϕ are considered to be the important performance parameters. Figure 4 shows the analytical results of the force ratio for section 3 at the exit plane (no diffuser) for various λ values. The analytical results of the entrained M_2 and exit Mach number M_3 are shown in Fig. 5. For the curve labeled $\lambda = 25$, the choked condition where $M_2 = 1$ occurs for $P_r \geq 9$. Hence, above this P_r the entrained mass flow is at the maximum which represents a limit on the suction force on the contoured inlet. At higher P_r beyond this condition, the force ratio degrades because of the choked limit. The M_3 continues to increase since the jet force increases at

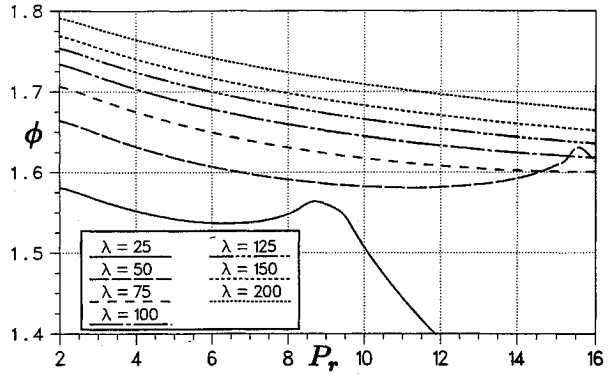

Fig. 4 Analytical results of force ratio for section 3 at exit plane.

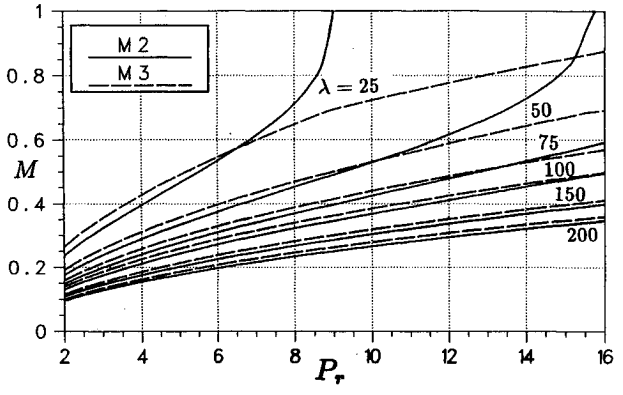

Fig. 5 Analytical results of entrained and exit Mach number vs P_r with section 3 at exit.

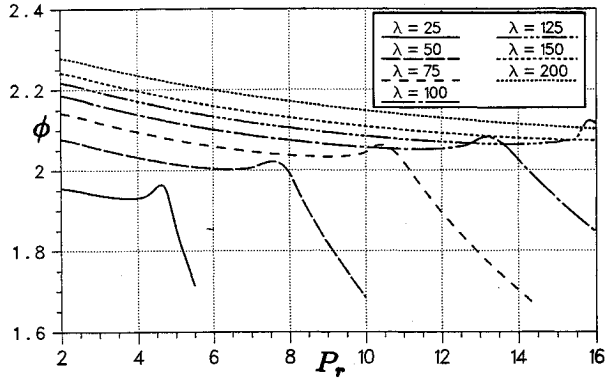

Fig. 6 Analytical results of force ratio for diffuser section 4 at exit plane $A_r = 1.67$, $L_s = 0.075$.

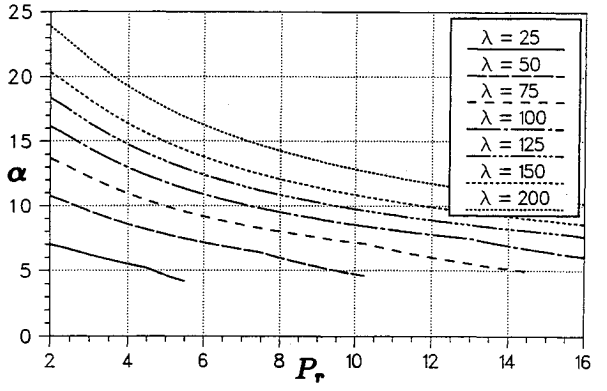

Fig. 7 Analytical results of mass ratio for diffuser section 4 at exit plane $A_r = 1.67$.

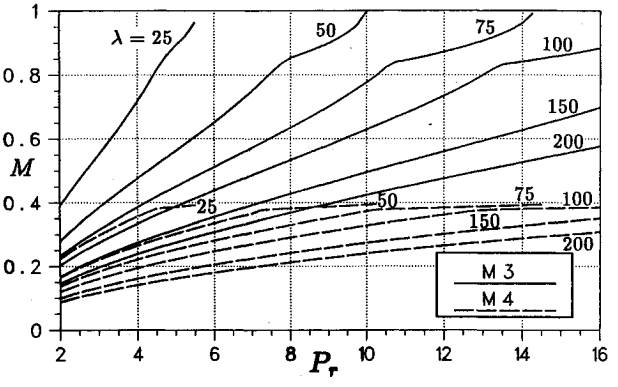

Fig. 8 Analytical results of M_3 and exit Mach number vs P_r with section 4 at exit.

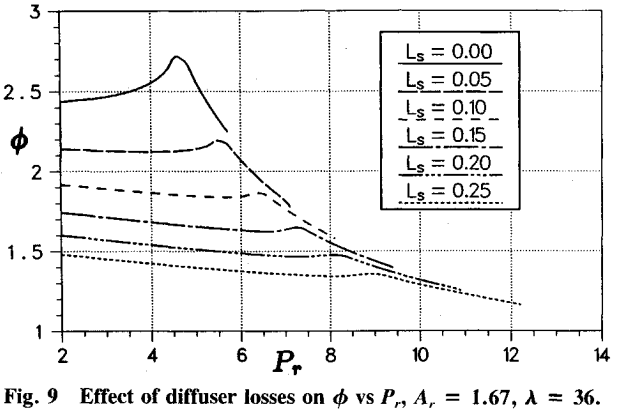

Fig. 9 Effect of diffuser losses on ϕ vs P_r, $A_r = 1.67$, $\lambda = 36$.

higher P_r values. Figure 6 shows the analytical results of force ratio for diffuser section 4 at the exit plane with a loss coefficient $L_s = 0.075$ for the diffuser and $A_r = 1.67$. The force ratio ϕ curves show a dramatic change in slope for P_r above the choked condition when $M_2 = 1$. Figure 7 shows the analytical results of the mass flow ratio for the diffuser section 4 at the exit plane. The diffuser data show that the choked limit for the entrance flow occurs at a lower P_r value. The corresponding analytical results for M_3 and the exit Mach number are shown in Fig. 8. The trends are similar to the straight section with a reduction in the exit Mach number. Figure 9 demonstrates the effect of diffuser losses, designated L_s from Eq. (7), on the ϕ vs P_r. As can be seen in Fig. 9, a small increase in the diffuser loss coefficient translates into a significant loss in total thrust. Therefore, the diffuser efficiency is an important aspect to overall ejector performance. These analytical results are considered to be the upper limit for the performance of the ejector design since complete mixing is implied for the one-dimensional analysis.

Ejector Component Forces

In this section a derivation of individual forces described in Fig. 3 will be undertaken in terms of the flow parameters at each station. The thrust augmentation of the ejectors studied in this investigation was a result of the suction force on the contoured inlet of the mixing chamber. The pressure integration from the wetted surface of the ejector from Eq. (10) leads to two components of force, the lip thrust F_l and diffuser drag F_d. Including the skin friction force F_{vx} and with the exit pressure at atmospheric, Eq. (10) reduces to

$$F_{tx} = F_l - F_d + F_{j1} - F_{vx} = \dot{m}_4 V_4 \tag{12}$$

Using the momentum equation in control volume form, the surface pressure integrals can be described as a force in terms of the thermodynamic variables. For a control volume encompassing ⓐ to ②, the force F_l shown in Fig. 3 from the pressure integration on the curved leading-edge section of the ejector is a unique function of the entrained Mach number, expressed as

$$\frac{F_l}{P_a A_3} = \left(1 - \frac{g}{\lambda}\right)\left[\frac{kM_2^2 + 1}{\left(1 + \dfrac{k-1}{2} M_2^2\right)^{k/(k-1)}} - 1\right] \tag{13}$$

The maximum possible value for the term in the brackets occurs when $M_2 = 1$, at the choked condition, which has a maximum value of 0.27 for air. Applying the conservation laws between stations ③ to ④, the pressure term from Eq. (10) on the diffuser walls leads to a force described in terms of the total pressure loss as

$$\frac{F_d}{P_a A_3} = (1 + A_r k M_4^2)\left[1 - (A_r)^{2k/(k+1)}\left(\frac{P_{t4}}{P_{t3}}\right)^{(k-1)/(k+1)} \times \left(\frac{M_4}{M_3}\right)^{2/(k+1)}\left(\frac{T_{t3}}{T_{t4}}\right)^{1/2}\left(\frac{1 + kM_3^2}{1 + A_r k M_4^2}\right)\right] \tag{14}$$

For the jet nozzle the flow can be considered to be isentropic and fully expanded to the local static pressure. For

$$\left(P_r \frac{P_a}{P_2}\right) > \left(\frac{2}{k+1}\right)^{-k/(k-1)}$$

that is greater than critical

$$\frac{F_{j1}}{P_a A_3} = \frac{P_r}{\lambda} k\left[\left(\frac{2}{k-1}\right)\left(\frac{2}{k+1}\right)^{(k+1)/(k-1)}\right]^{1/2} \times \left[1 - \left(\frac{P_1}{P_{t1}}\right)^{(k-1)/k}\right]^{1/2} + \frac{g}{\lambda}\left(\frac{P_2}{P_a} - 1\right) \tag{15}$$

The second term arises from the choice of control volume encompassing the jet exit area with the control surface projected upstream to the atmospheric plane namely, ⓐ to ①. The normalized skin friction force[15] is expressed as

$$\frac{F_{vx}}{P_a A_3} = \frac{P_2}{P_a}\frac{L_3}{D_3} k C_f M_2^2 \tag{16}$$

For a numerical estimate of C_f, the friction calculation from a developing turbulent boundary layer with zero presure gradient was averaged over the length for the straight portion of the ejector. Figure 10 shows the individual force components for $\lambda = 72$ for $A_r = 1.66$. The F_l thrust force reaches a maximum value when the entrained Mach number reaches one. For $\lambda = 72$ the flow is choked at $P_r = 10$ and the calculations were terminated when $M_3 = 1$.

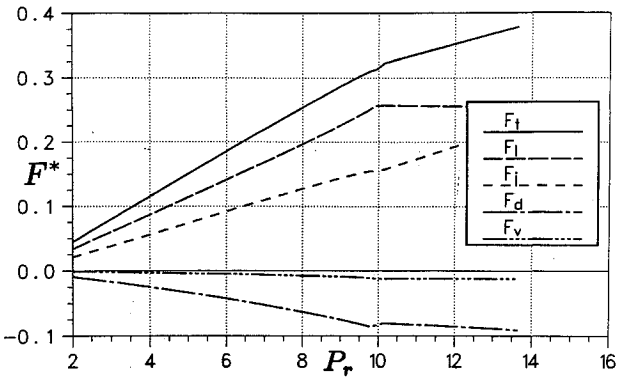

Fig. 10 Distribution of force components for ejector with diffuser, $A_r = 1.67$.

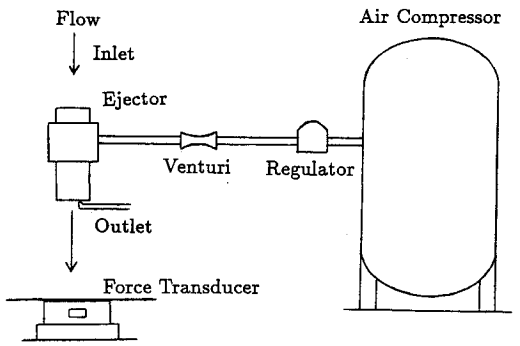

Fig. 11 Experimental arrangement for force measurement.

The analytical results for the ejector mixing show that specifying ideal ejector performance requires two independent geometric parameters. The performance has a functional dependence on the ejector area ratio $\lambda = (A_1/A_3)$ and the diffuser area ratio $A_r = (A_4/A_3)$, and increasing λ increases performance. These analytical results serve as a bench mark for performance and help to indicate the upper limit of thrust augmentation. The one-dimensional control volume methods provide the most simple analyses and are qualitatively valid since the turbulence mixing reduces the velocity gradients and the downstream flow approaches a uniform profile. Due to the complex three-dimensional nature of the expanding supersonic jet's interaction with the coflowing entrained air, an experimental procedure was adopted to ascertain the optimum length for this specific ejector configuration.

Experimental Results

Figure 11 shows the experimental arrangement for the force measurement of the ejector assembly. The force in the x direction was obtained by deflecting the axial momentum flux 90 deg from the ejector axis to recover the F_x component on a round plate fastened to a force balance. The ejector exit plane was positioned eight D_3 above the flat deflector plate which had a diameter of 1 m. A calibrated force transducer was utilized for the measurement of the axial force which is a direct measurement of the momentum flux. A rake of five static pressure probes was placed across the radius at the exit plane of the ejector to evaluate the mean static exit pressure which was used to evaluate the exit pressure term in Eq. (10) for the thrust. The value of the jet thrust F_{ja} used in the ϕ was calculated for a converging-diverging nozzle expanded fully to P_a and multiplied by the measured discharge coefficient. The actual nozzles were convergent to the exit plane, and therefore, would show some decline relative to the compressible flow analysis.

Figures 12 and 13 show the force augmentation ratio ϕ vs pressure ratio P_r for the straight and diffuser sections. The data with $\lambda = 72$ were obtained by plugging half of the primary nozzles. The overall force ratios are increased with $\lambda = 72$.

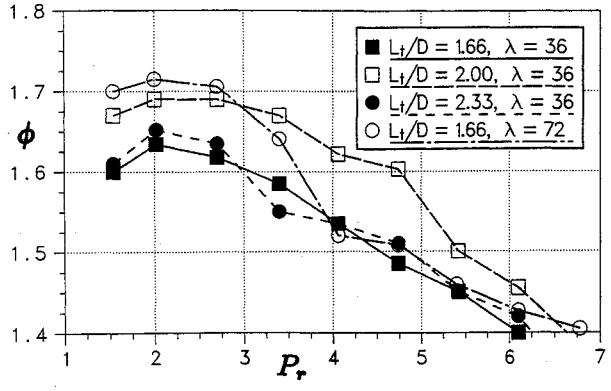

Fig. 12 Experimental ejector force to jet force ratio for $\lambda = 36$.

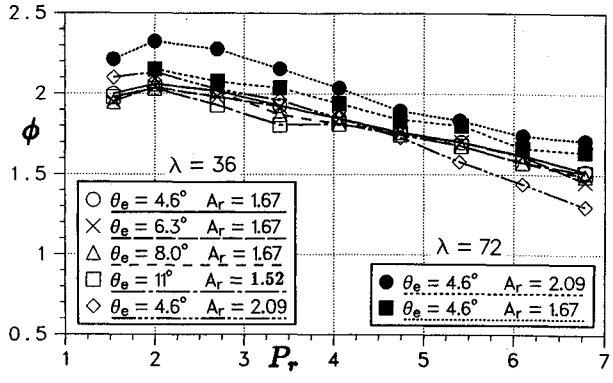

Fig. 13 Experimental ejector force to jet force ratio.

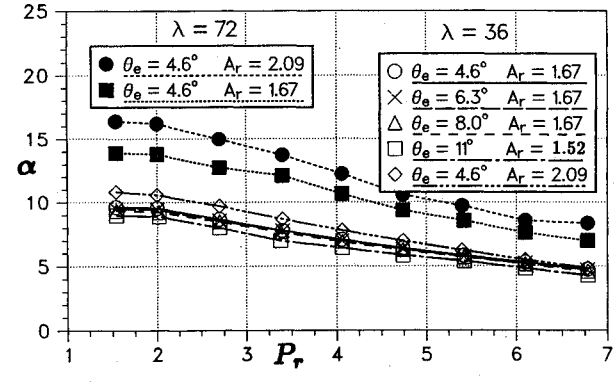

Fig. 14 Experimental ejector mass ratio vs P_r.

The force ratio has a maximum at $P_r \sim 2$ and decays at the higher P_r, partially due to incomplete mixing. The oblique wave propagation from the flow at the exit of the primary nozzles results in less turbulent mixing, degrading the performance at higher P_r values. Figure 12 supports the contention that mixing for the straight wall ejector is nearly complete, and performance maximized at an extension of $L_t/D_3 = 2.0$. Increasing the mixing duct length beyond two diameters actually degrades performance because the velocities at the edge of the boundary layer are higher when the flow is well-mixed and the resulting friction losses become more pronounced. For the straight section, the increase in the velocity ratio between the primary jet and the entrained air is responsible for a lower rate of turbulent mixing at the higher P_r, which results in a more nonuniform velocity profile at the exit plane.

Figure 13 shows a significant increase in force augmentation with the addition of a diffuser with augmentation increasing,

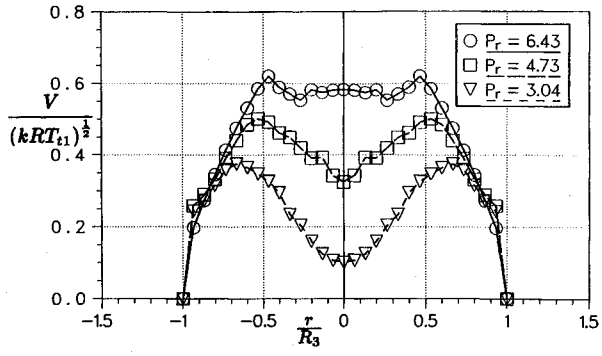

Fig. 15 Velocity profile at entrance to diffuser $L_3/D_3 = 1.0$, $A_r = 1.67$, $\lambda = 36$.

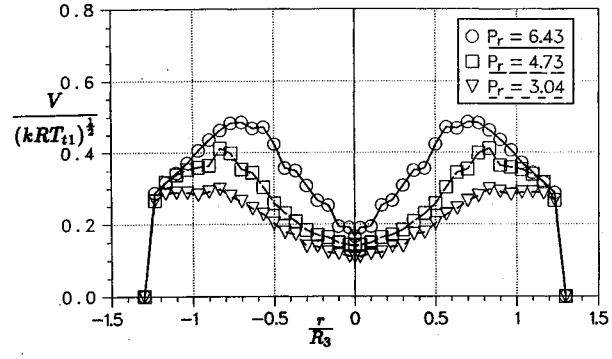

Fig. 16 Velocity profile at exit of diffuser $\theta = 4.6$ deg, $A_r = 1.67$, $\lambda = 36$.

with an increase in A_r for the lower P_r values. For the diffuser with $\theta_e = 11$ deg, the boundary layer remained attached for $\lambda = 36$ throughout the P_r range, which is attributed to the net circulation of the mixed flow controlling the boundary-layer separation. Figure 14 shows the corresponding induced mass entrainment ratio α for the diffuser combinations. The addition of the diffuser section shows a significant gain in both the force ratio and the induced mass through the inlet section of the ejector. The flow through the ejector with diffuser combination experiences a greater extraction of energy from the primary jet due to the expanding flow in the diffuser. Increasing the velocity ratio between the primary jet and entrained air for the flow in the diffuser results in an increased mixing rate. Figure 15 represents a plot of the measured velocity profiles at the exit plane of station ③ prior to the entrance of the diffuser. Figure 16 is the graphical representation of the velocity profile at the exit of the diffuser section with $\theta = 4.6$ deg and $A_r = 1.67$. These data were calculated from the total pressure readings from a miniature Keil probe and circumferential slotted static probe using the compressible flow equations. Surprisingly, the diffuser velocity profile shows a maximum value closer to the wall than the velocity profile of the straight section. At higher P_r, the side wall jets penetrate farther inward toward the centerline. The static pressure distribution at the exit of the diffuser is shown in Fig. 17 normalized by the atmospheric pressure. The static pressure gradient along the radius is the net result of the swirl induced by the primary jets, where centrifugal forces are balanced by the radial pressure gradient. The swirl has the net effect of diminishing the head losses in the diffuser section similar to the results in Ref. 16 where an upstream swirl was introduced with an increase in diffuser efficiency.

Incomplete Mixing

The factor β is a shape parameter associated with momentum distribution at a fixed plane of the ejector. The numeric value of $\beta = 1$ is the totally mixed or ideal conditions discussed

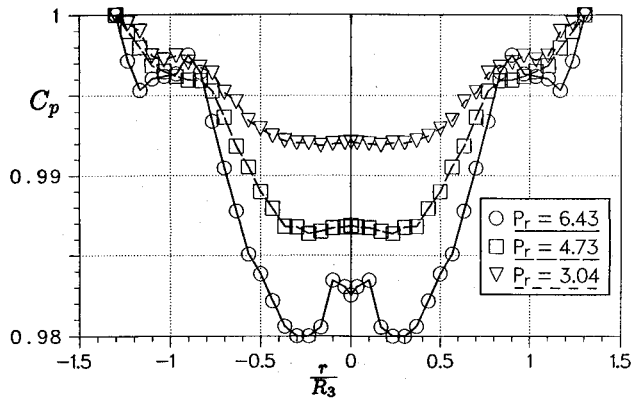

Fig. 17 Static pressure distribution at exit of diffuser, A_r = 1.67, λ = 36.

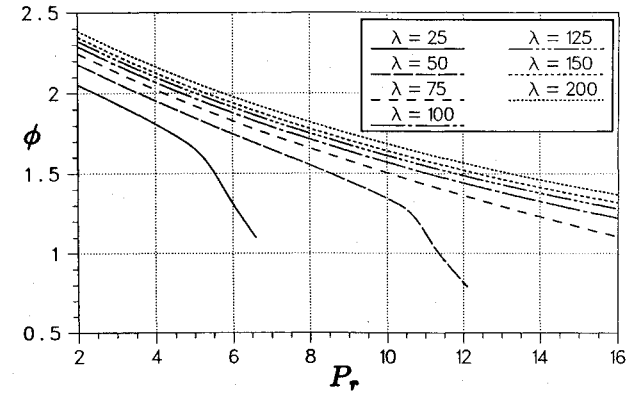

Fig. 18 Effect of incomplete mixing of ϕ vs P_r, A_r = 1.67, L_s = 0.05.

in the analytical formulation. For example, β_3 = 1 results from the perfectly uniform profiles characteristic of completely mixed flows, whereas β_3 = 1.33 for a parabolic velocity profile indicates large velocity excursions between primary and secondary streams. The momentum correction parameter was calculated as β_3 = 1.035 for L/D = 2.0 at a P_r = 3, and increased to β_3 = 1.06 at P_r = 6.8 without a diffuser attached. For the diffuser data, the measured β_4 = 1.09 did not vary significantly with P_r. However, at the inlet section to the diffuser, the momentum correction parameter β_3 = 1.04 at a P_r = 3 and increased to β_3 = 1.09 at P_r = 6.8, indicating a lower mixed condition at the inlet of the diffuser for the higher P_r.

The loss coefficient was measured for A_r = 1.67, λ = 36 by measuring the total pressure distribution at the inlet and exit of the diffuser using Eq. (7). The numerical value of the loss was L_s = 0.15 and was found to be independent of P_r. Since the mixing is simultaneously occurring in the diffuser length, the entropy increase is the result of both the jet mixing and the conventional diffuser loss. The loss in the diffuser independent of the mixing was calculated using the theoretical total pressure drop from stations ② to ③ which accounts for the entropy increase from the mixing alone. The diffuser loss deduced from this calculation varied from L_s = 0.045 to 0.055 for a P_r increasing from 3 to 6.5. The measured loss coefficient L_s and the corresponding β velocity shape parameter were incorporated in the momentum and entropy equation for the analysis. This represents a mathematical correction to the one-dimensional equations to extend the range of applicability for the analysis. The results are shown in Fig. 18 which incorporates a linear variation with β_3 increasing with P_r obtained from the measurement of the velocity and density profiles. The curves in Fig. 18 show the degradation of the force augmentation with increasing P_r from the influence of incomplete mixing.

Concluding Remarks

An experiment was undertaken to measure the mass entrainment and force augmentation capability of a multiple jet ejector. The data show that a large percentage increase of thrust can be realized for an ejector with multiple primary jets from the increased flow mixing rate downstream. The data for the ejector used in conjunction with an efficient diffuser demonstrate the best performance. The primary jet swirl imparts a net circulation to the combined flow which decreases the diffuser losses for large angle diffusers and demonstrates the efficient diffusion of the flow for this configuration. While more than a doubling of thrust is obtained, the calculations show that achieving such a goal demands extreme caution in controlling the loss mechanisms in the diffuser. Large angle diffusers show promise for increasing thrust augmentation with the constraint of minimum length. This investigation shows that λ and A_r are important parameters in increasing both the thrust and the mass augmentation ratio. Therefore, whenever possible, a larger mixing chamber combined with a low loss diffuser should be used for optimum efficiency. For larger A_r, the flow losses occurring in the diffuser begin to outweigh the benefits, and the ejector performance degrades. For increasing forward speed the ejector configuration should have the capability to revert from the angled diffuser configuration to the straight walled ejector during higher forward speeds to maintain a portion of the thrust augmentation.

Compressible control volume analyses were used to estimate the effect of geometric and fluid dynamic parameters on performance. The control volume equations demonstrate the performance trends for an ejector operating under different primary pressures. The numerical analysis provides insight into interactions between the geometric parameters and provides an upper limit for ejector performance. Control volume methods, however, fail to account for the interaction between the state variables and the heart of the ejector process, namely turbulent mixing. Their shortcoming is their inability to describe physical events in terms of the length scales to provide for complete mixing. However, the inclusion of incomplete mixing effects through the insertion of the experimentally measured shape parameter β in the momentum equation provides for a global correction for the turbulent mixing in the analysis. The compressible flow control volume analyses with the experimentally corrected shape parameters and loss coefficients provide insight to the thermodynamic limits of ejector performance with a diffuser.

Acknowledgment

This research was partially funded through the Wright State University Research Incentive Program.

References

[1]Von Karman, T., "Theoretical Remarks on Thrust Augmentation," Reissner Anniversary Volume, Contribution to *Applied Mechanics*, 1949.

[2]Alperin, M., and Wu, J., "Thrust Augmenting Ejectors, Part I," *AIAA Journal*, Vol. 21, No. 10, 1983, pp. 1428–1436.

[3]Fabri, J., and Siestrunck, R., "Supersonic Air Ejectors," *Advances in Applied Mechanics*, Vol. 5, Sec. 1, Academic Press, New York, 1958, pp. 1–34.

[4]Bevilaqua, P. M., "Evaluation of Hypermixing for Thrust Augmenting Ejectors," *Journal of Aircraft*, Vol. 11, No. 6, 1973, pp. 348–354.

[5]Quinn, B., "Ejector Performance at High Temperatures and Pressures," *Journal of Aircraft*, Vol. 13, Dec. 1976.

[6]Quinn, B., "Effects of Aeroacoustic Interactions on Ejector Performance," *Journal of Aircraft*, Vol. 12, Nov. 1975.

[7]Quinn, B., "Recent Developments in Large Area Ratio Thrust Augmentors," AIAA Paper 72-1174, 1972.

[8]Quinn, B., "Ejector Performance at High Temperatures and Pressures," *Journal of Aircraft*, Vol. 13, No. 12, 1976, pp. 948–954.

[9]Quinn, B., "Thrust Augmenting Ejectors: A Review of the Application of Jet Mechanics to V/STOL Aircraft Propulsion," AGARD

CP-308, Nov. 1981.

[10]Porter, J. L., and Squyers, R. A., "A Summary/Overview of Ejector Augmentor Theory and Performance," Vought Corp. Advanced Technology Center, ATC Rept. R-91100/9CR-47A, Dallas, TX, April 1981.

[11]Dutton, J. C., "Investigations of the Supersonic-Supersonic Ejector," *Proceedings of the Ejector Workshop for Aerospace Applications*, Dayton, OH, Aug. 1981.

[12]Yang, T., Ntone, F., Jiang, T., and Pitts, D. R., "An Investigation of High Performance, Short Thrust Augmenting Ejectors," *Journal of Fluids Engineering*, Vol. 107, March 1985.

[13]Krothapalli, A., Van Dommelen, L., and Karamcheti, K., "The Influence of Forward Flight on Thrust Augmenting Ejectors," AIAA Paper 85-1589, July 1985.

[14]Oates, G. C., *Aerothermodynamics of Gas Turbine and Rocket Propulsion*, AIAA Education Series, AIAA, Washington, DC, 1988, pp. 38–53, 166–168.

[15]Shapiro, A. H., *The Dynamics and Thermodynamics of Compressible Fluid Flow*, Vol. 1, Wiley, New York, 1953, pp. 220–240.

[16]McDonald, A. T., and Van Dewoestine, R. V., "Effects of Swirling Inlet Flow on Pressure Recovery in Conical Diffusers," *AIAA Journal*, Vol. 9, No. 10, 1971.